

# Effects of incomplete remediation of NAPL-contaminated aquifers: experimental and numerical modeling investigations

Schradh Saenton · Tissa H. Illangasekare

Received: 31 July 2012 / Accepted: 8 February 2013 / Published online: 26 February 2013  
© The Author(s) 2013. This article is published with open access at Springerlink.com

**Abstract** The benefits of partial source zone treatment of non-aqueous phase liquids (NAPL)-contaminated sites (not fully removing the entrapped free-phase NAPL sources) with respect to achieving cleanup goals and reducing concentrations of dissolved constituents in downstream plumes are being debated. Uncertainty associated with the removal of NAPLs from source zones could be attributed to a number of factors including lack of information on the extent or timing of spills, complex entrapment configurations created by unstable behavior (fingering), geologic heterogeneity, and unavailability of accurate techniques for characterizing these heterogeneities, and uncertainty in locating source zone and estimating NAPL mass. Data for the resolution of issues related to benefits of partial source zone treatment are not expected to come from field sites. Laboratory studies in intermediate-scale test tanks can provide accurate data sets to investigate this issue, as it is possible to conduct controlled experiments under known conditions of aquifer heterogeneity. At this scale, source depletion and downstream concentrations in dissolved plumes can be monitored during remediation. The data generated in controlled experiments are used to validate numerical models to conduct theoretical analysis. This

paper discusses this approach and presents results from such a study where the benefits of partial source zone treatment using surfactants were evaluated using intermediate-scale testing and numerical modeling. Results from both experiment and numerical simulations agreed conceptually where they suggested that a very large fraction of NAPL has to be removed from the entrapment zone to significantly reduce downstream plume concentrations.

**Keywords** Dissolution · DNAPL · Heterogeneity · Numerical modeling · Surfactants

## Abbreviations

$b$	Sorption parameter in the Langmuir isotherm ( $L^3 M^{-1}$ )
$c$	Aqueous concentration ( $M L^{-3}$ )
$c^*$	Apparent aqueous solubility of PCE in the presence of Tween-80 ( $M L^{-3}$ )
$c_s$	Aqueous solubility of PCE under normal condition (i.e., no surfactant) ( $M L^{-3}$ )
$c_{tw}$	Aqueous concentration of Tween-80 ( $M L^{-3}$ )
$d_{50}$	Average grain size (L)
$D_m$	Molecular diffusion coefficient ( $L^2 T^{-1}$ )
$J$	NAPL-water mass transfer rate per unit volume of porous medium ( $M L^{-3} T^{-1}$ )
$k_{La}$	Overall mass transfer coefficient ( $T^{-1}$ )
$k_{r,w}$	Relative permeability of water in the sand (—)
$K$	Effective hydraulic conductivity ( $L T^{-1}$ )
$K_s$	Saturated hydraulic conductivity ( $L T^{-1}$ )
$\overline{\ln K_s}$	Average of (natural) log of $K_s$
$L^*$	Characteristic or dissolution length (L)
$m_0$	Original PCE mass in the source zone
$Pe$	Peclet number (—)
$Re$	Reynolds number (—)

S. Saenton (✉)  
Department of Geological Sciences, Faculty of Science,  
Chiang Mai University, Chiang Mai 50200, Thailand  
e-mail: ssaenton@gmail.com; schradh.saenton@cmu.ac.th  
URL: <http://ssaenton.geol.science.cmu.ac.th>

T. H. Illangasekare  
Division of Environmental Science and Engineering, Center  
for Experimental Study of Subsurface Environmental Processes  
(CESEP), Colorado School of Mines, Golden, CO 80401, USA  
e-mail: [tillanga@mines.edu](mailto:tillanga@mines.edu)  
URL: <http://cesep.mines.edu>

$s$	Fraction of sorbed mass ( $M M^{-1}$ )
$s_{\ln K_s}^2$	Variance of (natural) log of $K_s$
$S_n$	PCE saturation (–)
$\bar{S}_n$	Average PCE saturation (–)
$S_{r,w}$	Residual water saturation (–)
$S_w$	Water saturation (–)
Sc	Schmidt number (–)
Sh	Modified Sherwood number (–)
Sh <sub>N</sub>	Modified Sherwood number for natural dissolution (–)
Sh <sub>E</sub>	Modified Sherwood number for surfactant-enhanced dissolution (–)
$\Delta m_i$	The amount of PCE mass removed from the source zone after application of surfactant injection of time $\Delta t_i$ (M)
$\Gamma_{\max}$	Sorption parameter in Langmuir isotherm ( $M M^{-1}$ )
$\theta_n$	Volumetric NAPL content (–)
$\tau$	Tortuosity factor (–)

## Introduction

Non-aqueous phase liquids (NAPLs) such as gasoline and chlorinated solvents are common organic pollutants found in contaminated soils and aquifers (Mercer and Cohen 1990). These organic liquids often are entrapped in the subsurface where they slowly dissolve into flowing groundwater and generate downstream contaminant plumes in which concentrations exceed regulatory standards. Although several technologies have been proposed recently for NAPL cleanup, the ability to completely remediate these contaminated sites is still in doubt. Such uncertainty is not only caused by the ineffectiveness of the remediation technique, but could also be attributed to the unavailability of methods for characterizing aquifer heterogeneities and the inability to accurately characterize the saturation distribution of NAPL in the source zone. These factors result in errors in both locating and estimating volume of NAPL in the source zone. Consequently, complete removal of NAPL mass from the source zone may become impossible or impractical using any available cleanup technology.

Geologic heterogeneity is one of the primary factors that controls migration and distribution of NAPL in the subsurface (Kueper et al. 1989; Kueper and Frind 1991; Kueper and Gerhard 1995; Illangasekare et al. 1995; Illangasekare 1998; Dekker and Abriola 2000; Bradford et al. 2000). It also complicates characterization of the source zone (Nelson et al. 1999) and effectiveness of NAPL remediation (Ewing 1996; Meinardus et al. 2002; Saenton et al. 2002). Saenton et al. (2002) demonstrated that uncharacterized aquifer heterogeneity can cause significant uncertainty in the removal of

NAPL from source zones. In that study, the effectiveness of surfactant-enhanced aquifer remediation (SEAR) for removal of *p*-xylene-contaminated soils in heterogeneous formations was investigated. A numerical model, validated using data generated in test tanks, was used to simulate mass removal during surfactant injection. Analysis of numerical model results showed that the required cleanup time depends on how NAPL is distributed in the source zone after a spill. The distribution of entrapped NAPL is referred to in this paper as entrapment architecture. In some cases, some of the entrapped NAPL was not removed even after long treatment periods because the treating reagents (e.g., surfactants) completely bypassed low permeability zones. Conventional pump-and-treat remediation methods have been found to be ineffective in removing significant NAPL mass due to low rates of natural dissolution. Remediation engineers have now focused on more aggressive NAPL removal technologies such as enhanced bioremediation, in situ chemical oxidation, co-solvent flushing, and SEAR which is of interest in this work.

Sale and McWhorter (2001) point out the limited near-term benefits of partial source zone treatment in achieving cleanup goals with expected reduction of dissolved contaminant concentrations downstream of the source zone. They conclude that mass removal from source zones is ineffective unless a large fraction of the entrapped free-phase NAPL is removed.

Sale and McWhorter (2001) study however considered only very simplified source architecture and flow conditions. These simplifications included uniform flow fields, simple entrapment architecture that consisted of only NAPL pools and a dissolution model that did not allow for changes in NAPL saturation. Hence, it may be premature to generalize the applicability of their findings to field sites that produce complex NAPL entrapment configurations and non-uniform flow fields under heterogeneous conditions.

This paper further investigates this issue by considering the application of SEAR technology that may only partially remove free-phase NAPL from a heterogeneous source zone. Analysis is conducted at intermediate scales using two-dimensional (2-D) test tanks to create heterogeneous systems with complex entrapment architecture and non-uniform flow fields. Concentrations in the downstream dissolved plume, which are a function of mass depletion rate or the amount of NAPL mass left in the source zone, are monitored and the consequences of incomplete source zone treatment are evaluated.

## Background

### Dissolution of non-aqueous phase liquids

Based on methods developed in chemical engineering, a linear-driving force model for mass transfer from

entrapped NAPLs in soils has been proposed (Miller et al. 1990) and it is expressed as:

$$J = -k_{La}(c - c^*), \quad (1)$$

where  $J$  ( $\text{M L}^{-3} \text{T}^{-1}$ ) is a dissolved mass flux due to dissolution of NAPL per unit volume of porous medium, and  $c$  and  $c^*$  are dissolved concentration and *apparent* aqueous solubility [ $\text{M L}^{-3}$ ], respectively. The value of  $k_{La}$  [ $\text{T}^{-1}$ ] is usually calculated based on correlations containing a modified form of dimensionless Sherwood number (Sh):  $k_{La} = D_m \text{Sh}/d_{50}^2$  where  $D_m$  and  $d_{50}$  are aqueous phase molecular diffusion coefficient [ $\text{L}^2 \text{T}^{-1}$ ] and average grain size diameter [L], respectively. For simple flow systems, it is possible to derive the relationship between the Sherwood number and other dimensionless groups such as Reynolds ( $Re$ ), Schmidt ( $Sc$ ), or Peclet ( $Pe$ ) numbers. These functional relationships are referred to as Gilland-Sherwood models. A number of similar system-specific empirical relationships have been proposed for NAPL dissolution (Miller et al. 1990; Powers et al. 1992; Imhoff et al. 1994). Lumped mass transfer coefficients, that are estimated using the modified Sherwood number, quantify the mass transfer that occurs at the representative elementary volume (REV) scale, a scale that is larger than the pore scale where mass transfer occurs at the NAPL/water interfaces. Saba and Illangasekare (2000) suggested a Gilland-Sherwood model for *natural* dissolution that is scale dependent and can account for dimensionality. The relationship is given as:

$$\text{Sh}_N = \alpha_1 (Re)^{\alpha_2} (Sc)^{\alpha_3} \left( \frac{\theta_n d_{50}}{\tau L^*} \right)^{\alpha_4}. \quad (2)$$

The constants  $\alpha_1, \alpha_2, \dots, \alpha_4$  are empirical fitting parameters. These parameters are usually obtained by fitting a model such as the one given by Eq. (2) to data generated from dissolution experiments conducted in a controlled one-dimensional (1-D) column or 2-D cell experiments.  $\theta_n$  is the volumetric NAPL content which is equal to the product of NAPL saturation ( $S_n$ ) and porosity ( $\phi_0$ ). The parameter  $\tau$  is tortuosity factor which is obtained from fitting a 1-D contaminant transport model (analytical solution) to the conservative tracer breakthrough curve data obtained from the column experiment. The value of tortuosity factor for sands used in this experiment is in the range of 1.8–2.2 (Saba 1999).  $L^*$  is the dissolution length which corresponds to the distance that aqueous phase flows through the NAPL zone. In a finite-difference model,  $L^*$  is the length a numerical grid block in the principal groundwater flow direction. For example, if the groundwater flow direction in a numerical grid block is mainly in the  $x$ -direction (i.e.,  $|v_x| > |v_y|, |v_z|$ ), the dissolution length will be  $L^* = \Delta x$  for that grid block. Thus, in a heterogeneous

flow field, the value of  $L^*$  can vary from one location to another.

Although 1-D column experiments provide a fundamental understanding of the processes or parameters that govern mass transfer, it is necessary to have a dissolution model that can account for the effect of flow bypassing (Saba and Illangasekare 2000) as well as scale dependency on mass transfer (Saba 1999; Nambi and Powers 2000; Schaerlaekens and Feyen 2004). Saba and Illangasekare (2000) demonstrated that neglecting the dimensionality of the flow field can result in orders of magnitude errors in estimates of mass transfer coefficients using these empirical relationships. Therefore, in this study, the dissolution model is calibrated with a 2-D experiment and is used in subsequent numerical modeling investigation.

### Enhanced dissolution using surfactants

A number of laboratory studies have demonstrated that surfactants can effectively remove entrapped DNAPLs from contaminated soils (Fountain et al. 1991; Pennell et al. 1993; McCray and Brusseau 1998; McCray et al. 2001). Surfactant-enhanced NAPL recovery has also been implemented at field sites, which in some cases have produced promising results (Abdul et al. 1992; Martel et al. 1998).

In many surfactant-flushing studies, it has been shown that the efficiency of remediation is largely affected by the rate-limited dissolution of organic constituents from NAPL (Pennell et al. 1993; Pennell et al. 1994; Mason and Kueper 1996). The dissolution rate can be quantified using similar laboratory and modeling procedures that were used in the development of correlations for natural dissolution. Examples of the relationship include the work done by Saba et al. (2001); Schaerlaekens and Feyen (2004) and Rathfelder et al. (2001). Saba et al. (2001) shows surfactant-enhanced NAPL dissolution as:

$$\text{Sh}_E = \beta_1 (Re)^{\beta_2} (Sc)^{\beta_3} \left( \frac{\theta_n}{1 - \theta_n} \right)^{\beta_4} \left( \frac{d_{50}}{\tau L^*} \right)^{\beta_5}, \quad (3)$$

where the empirical parameters  $\beta_1, \beta_2, \dots, \beta_5$  appearing in the above expression are usually determined by fitting experimental data of enhanced dissolution to the numerical model through inverse modeling.

Equations (2) and (3) are used to describe natural and enhanced dissolution of entrapped DNAPL.

### DNAPL mass removal in the upscaled domain

The removal of entrapped DNAPL either from natural or enhanced dissolution in the upscaled domain has been investigated through numerical modeling study by several

researchers in recent years (Parker and Park 2004; Park and Parker 2005; Grant et al. 2007; Saenton and Illangasekare 2007; Maji and Sudicky 2008; Basu et al. 2008). Among these studies, Parker and Park (2004) and Park and Parker (2005) proposed and verified an upscaled dissolution model where the temporal downstream concentration as well as mass flux from the entrapped DNAPL were a function of average groundwater velocity and, more importantly, a function of the ratio between DNAPL mass at any time to the original spilled mass to some power or  $(M/M_0)^\beta$ . Saenton and Illangasekare (2007), on the other hand, developed an upscaled natural dissolution model which considered soil's heterogeneity (in terms of variance of  $\ln K$ ), spatial distribution and spreading of DNAPL mass in the source zone (in terms of spatial moment), and a dissolution length (Saba and Illangasekare 2000). These methods, of course, require intensive amount of data acquisition which sometimes cannot be obtained from the field investigation.

Several simple, but very powerful, relationships for predicting mass flux (and/or concentration) based on the amount DNAPL mass left in the source zone have been proposed by several studies (Falta et al. 2005; Brusseau et al. 2008; DiFilippo and Brusseau 2011). These relationships enable the first estimation of mass flux (or concentration) without having to rely on massive site data except for the geometry or the distribution of DNAPL in the entrapment zone (e.g., GTP or ganglia-to-pool ratio).

## Numerical models

### NAPL migration model

The development of many multiphase flow models has been reported (Kaluarachchi and Parker 1990; Sleep and Sykes 1993; Delshad et al. 1996; Dekker and Abriola 2000). In general, these models are designed to solve a coupled set of partial differential equations representing two-phase flow in porous media. An example model is UTCHEM (Delshad et al. 1996), which is a 3-D, multi-component, compositional finite-difference simulator for multiphase flow and contaminant transport in porous media.

### Natural and enhanced dissolution model

The numerical models used to simulate mass transfer processes are based on modifications of existing flow and transport codes. MODFLOW (Harbaugh et al. 2000), a U.S. geological survey (USGS) finite-difference groundwater flow model, is used to simulate groundwater flow, whereas the reactive transport code RT3D (Clement 1997)

with the implemented NAPL dissolution module is used to simulate the transport of chemical species. The dissolution module is incorporated into the existing RT3D code as an additional reaction package that is designed to solve Eq. (1). Transient mass transfer simulation is achieved using a series of piecewise steady-state simulations. Velocity fields obtained from MODFLOW using effective hydraulic conductivity field,  $K$  (see below for description of this parameter), as a result of NAPL entrapment, is used in RT3D within the dissolution module (DSS) to simulate mass transfer with given effective porosity and NAPL saturation. The simulation sequence is repeated until the target time is reached with the updated values of NAPL saturation, porosity, and effective hydraulic conductivity. Such repeated execution loops are made possible using Perl scripts. A flowchart of simulation procedures and execution sequences of program modules is given in Fig. 1. A more detailed description of the model algorithms can be found in Saenton (2003).

The effective hydraulic conductivity,  $K$ , can be expressed in terms of relative permeability,  $k_{r,w}$ , and saturated hydraulic conductivity,  $K_s$  as:

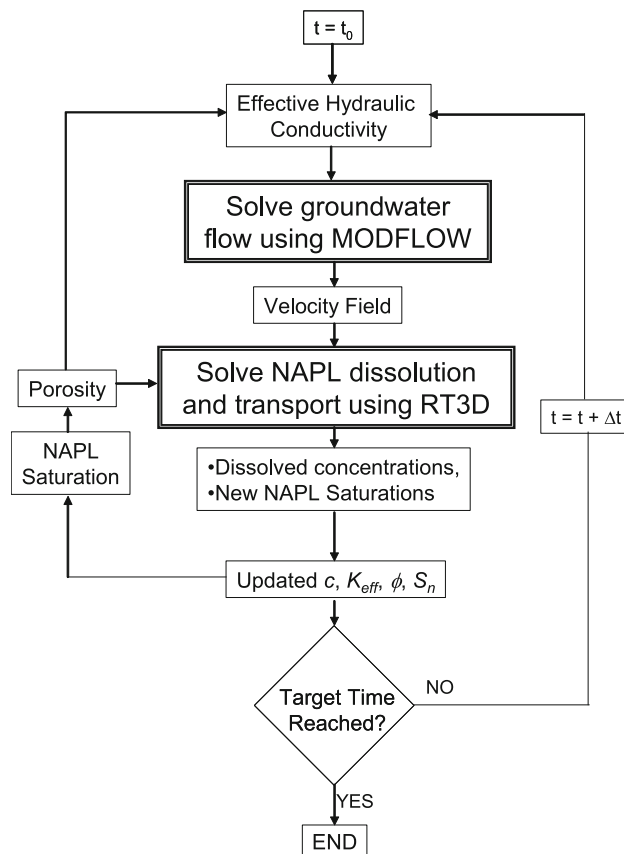


**Fig. 1** A flowchart showing simulation procedures and execution sequences of program units

$$K = k_{r,w}K_s \quad (4)$$

The relative permeability is a function of water saturation or  $k_{r,w} = k_{r,w}(S_w)$ . Several expressions of this function have been proposed by Wyllie (1962); Brooks and Corey (1966) and van Genuchten (1980). The numerical model developed in this study has the flexibility to use experimentally derived relative permeability functions. In this study, Wyllie's equation (1992) was chosen because it was found to best describe the relative permeability measurement data for the test sands used in our laboratory investigations (Saba 1999; Saba and Illangasekare 2000). Wyllie's equation is given as:

$$k_{r,w} = \left( \frac{1 - S_n - S_{r,w}}{1 - S_{r,w}} \right)^3, \quad (5)$$

where  $S_n$  and  $S_{r,w}$  are NAPL and residual water saturations, respectively.

## Experiments

Natural and surfactant-enhanced dissolution experiments were conducted in a bench-scale, 2-D horizontal dissolution cell containing a NAPL source in the middle of the tank. The purpose of these experiments was to obtain natural and surfactant-enhanced dissolution datasets necessary for model calibration and validation. The validated numerical models were then used to conduct theoretical analyses on the dissolution of NAPL in heterogeneous aquifers.

### Materials

The test DNAPL used in this research is tetrachloroethene or PCE. This test chemical is selected for this research because it has sufficiently slow (i.e., measurable) dissolution kinetics as well as low aqueous solubility compared to another well-known DNAPL compound, trichloroethene (TCE). A single component of DNAPL was used to eliminate the experimental and interpretive complications arising due to the effects of variable composition. Because pure tetrachloroethene is colorless, it was dyed red with Sudan IV (Sigma Chemicals) for visual identification. The physicochemical properties of PCE are listed in Table 1.

The surfactant used in this research was polyoxyethylene (20) sorbitan mono-oleate, commercially known as Tween-80 (Aldrich Chemicals). It is a non-toxic and biodegradable food-grade additive used in the food and pharmaceutical industries. Tween-80 was used in the enhanced dissolution because of its low critical micelle concentration. The properties of Tween-80 are listed in Table 2. Batch experiments were also conducted to confirm

**Table 1** Properties of tetrachloroethene or PCE at 25 °C

Properties	Value	Unit
Chemical formula	C <sub>2</sub> Cl <sub>4</sub>	–
Molecular weight <sup>a</sup>	165.8	g mol <sup>-1</sup>
Density <sup>a</sup>	1.62	g cm <sup>-3</sup>
Aqueous solubility <sup>b</sup>	200	mg L <sup>-1</sup>
Diffusion coefficient <sup>b</sup>	$8.19 \times 10^{-10}$	m <sup>2</sup> s <sup>-1</sup>
Viscosity	<1	cp
MCL	0.005	mg L <sup>-1</sup>

<sup>a</sup> Lucius et al. (1992)

<sup>b</sup> US EPA (1996)

**Table 2** Properties of Tween-80 (surfactant)

Properties	Value	Unit
Average molecular weight	1310.0 <sup>a</sup>	g mol <sup>-1</sup>
Density (5 %)	1.064 <sup>b</sup>	g cm <sup>-3</sup>
Dynamic viscosity (5 %)	1.117 <sup>b</sup>	cp
CMC	13.0 <sup>a</sup>	mg L <sup>-1</sup>

<sup>a</sup> Pennell et al. (1993)

<sup>b</sup> Ewing (1996)

the potential of Tween-80 to enhance PCE solubilization. An expression for enhanced dissolution was derived from experimental data (not shown) by fitting a linear model given as:

$$\frac{c^*}{c_s} = 1.0 + (2.30 \times 10^{-3}) c_{tw}, \quad (6)$$

where  $c^*$  is the apparent aqueous solubility of PCE [M L<sup>-3</sup>],  $c_s$  is the aqueous solubility of PCE under normal condition which is 200 mg L<sup>-1</sup>, and  $c_{tw}$  is aqueous concentration of surfactant Tween-80 in mg L<sup>-1</sup>. Batch tests were conducted to obtain sorption parameters between the chemicals and media used in the experiments (Saenton 2003). Properties of the five sands used in the experiments and numerical simulation studies are listed in Table 3.

### Dissolution experiments

#### 2-D horizontal dissolution cell

Dissolution experiments were conducted in a bench-scale, 2-D horizontal dissolution cell containing NAPL source(s) in the center of the cell (Fig. 2). The purpose of this experiment was to obtain data for the dissolution model calibration. The test cell consisted of clear plexiglass walls for the top and bottom plates and aluminium for the side plates. Internal void dimensions of the tank were nominally 65 cm long by 45 cm high by 5 cm wide.

**Table 3** Properties of sands used in the experiments and numerical simulation studies

Sand sieve sizes	$K_s (\times 10^{-3} \text{ m s}^{-1})^a$	$d_{50} (\times 10^{-3} \text{ m})$ (Unimin Corp.)	$S_{r,w} (-)^a$	PCE sorption, $K_d (\text{L kg}^{-1})$	Surfactant sorption (Langmuir isotherm) <sup>c</sup>	
					$\Gamma_{\text{max}} (\text{kg kg}^{-1})$	$b (\text{L kg}^{-1})$
#16	8.03	1.08	0.07	1.53 <sup>b</sup>	$9.1 \times 10^{-3b}$	42.6 <sup>b</sup>
#30	1.98	0.50	0.26	1.04 <sup>d</sup>	$6.0 \times 10^{-3d}$	1.04 <sup>d</sup>
#50	0.406	0.32	0.29	1.27 <sup>d</sup>	–	–
#70	0.243	0.20	0.30	1.52 <sup>b</sup>	$8.7 \times 10^{-3b}$	42.5 <sup>b</sup>
#110	0.053	0.12	0.26	1.33 <sup>d</sup>	–	–

<sup>a</sup> Compos (1998) and Saba (1999)

<sup>b</sup> Saenton (2003)

<sup>c</sup>  $s = \Gamma_{\text{max}} bc / (1 + bc)$

<sup>d</sup> Unpublished values

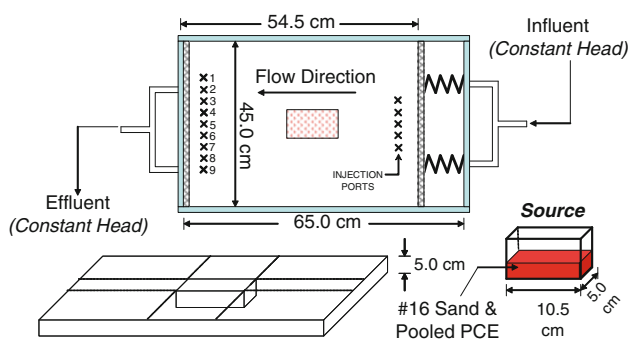


**Fig. 2** Two-dimensional, bench-scale dissolution cell with one PCE source

The test cell was filled with sand to form a simple heterogeneous system that consisted of a coarse sand lens surrounded by finer sand (Fig. 2). In this case, coarse and fine sands were used with mesh sizes #16 and #70, respectively.

For this experiment, the source size was 10.5 cm long and 5.0 cm wide and 5.0 cm high (Fig. 2). The initially water-wet source zone was filled to approximately one-third of total source thickness with red-dyed (Sudan IV, Sigma Chemicals) tetrachloroethene or PCE (Aldrich Chemicals). A volume of  $31.0 \text{ cm}^3$  PCE was injected into the source zone using a glass syringe under no flow conditions. PCE was injected into the source zone through 15 equally spaced injection ports located on the top of the test tank. The tank was then flipped over to allow the injected PCE to be entrapped in the source zone. After 2 days, the tank was flipped back allowing PCE to sink due to gravity for 24 h. In this way, a fully developed saturation profile was generated where NAPL saturation ranged from residual in the upper part of the source zone to high saturation at the bottom of the source zone.

Constant head reservoirs were installed upstream and downstream of the test cell to maintain a continuous and

steady flow of deionized water (ROPure<sup>®</sup>, Barnstead-Thermolyne Corporation) through the test cell. An array of five injection ports located upstream of the source zone was installed for use in enhanced dissolution experiments. A multi-channel syringe pump (Soil Measurement Systems) was used to provide a constant injection rate for the surfactant solution. Nine sampling ports located downstream were used to extract aqueous solution samples. The effluent port was used as an additional sampling port to monitor both total flow rate and mass balance. It should be noted that these experiments were conducted without replicate due to the difficulty in reproducing identical NAPL saturation profile.

### Natural dissolution

A series of dissolution experiments were conducted for both transient and steady-state conditions in the dissolution cell. A hydraulic gradient of approximately  $10^{-2}$  ( $\Delta h = 0.54 \text{ cm}$ ) was applied to the test cell producing the flow rate of  $3.25 \text{ cm}^3 \text{ min}^{-1}$ , while PCE concentrations were monitored at downstream ports and in the fully mixed tank effluent. Figure 3 shows the examples of transient PCE concentration at port #5 and the effluent. Typical transient breakthrough curves of NAPL dissolution were characterized by a rise in concentration from zero or the background value at the dissolution front followed by a plateau at steady-state concentration. The highest steady-state concentration ( $117.0 \text{ mg L}^{-1}$ ) was observed at the central port of the sampling array (port #5). Dissolved PCE in the effluent reached a steady-state value of  $27.0 \text{ mg L}^{-1}$ .

The steady-state concentration of PCE was monitored at several groundwater flow rates. Different hydraulic gradients ranging between approximately  $4.3 \times 10^{-3}$  and  $2.7 \times 10^{-2}$  were applied to the dissolution cell to produce steady-state flow rates ranging from 1.4 to  $9.0 \text{ cm}^3 \text{ min}^{-1}$ .

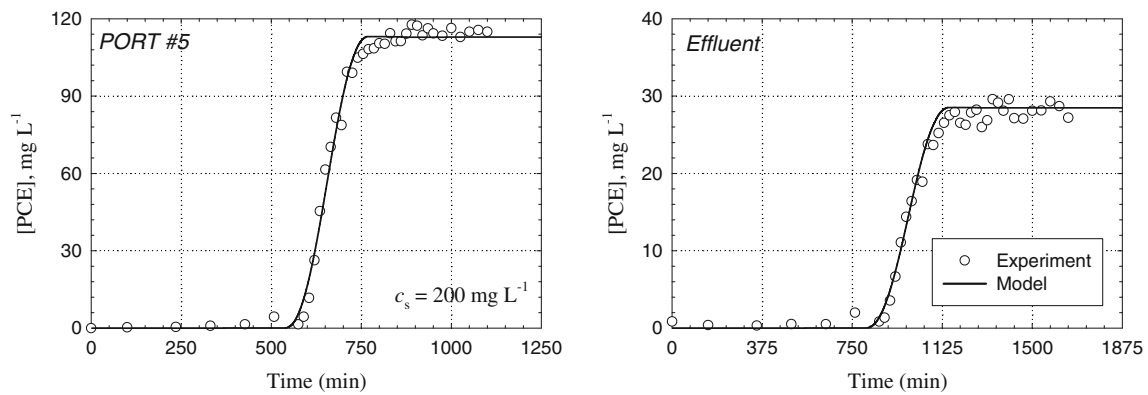


**Fig. 3** Transient dissolution of PCE: experimental data and model simulated values

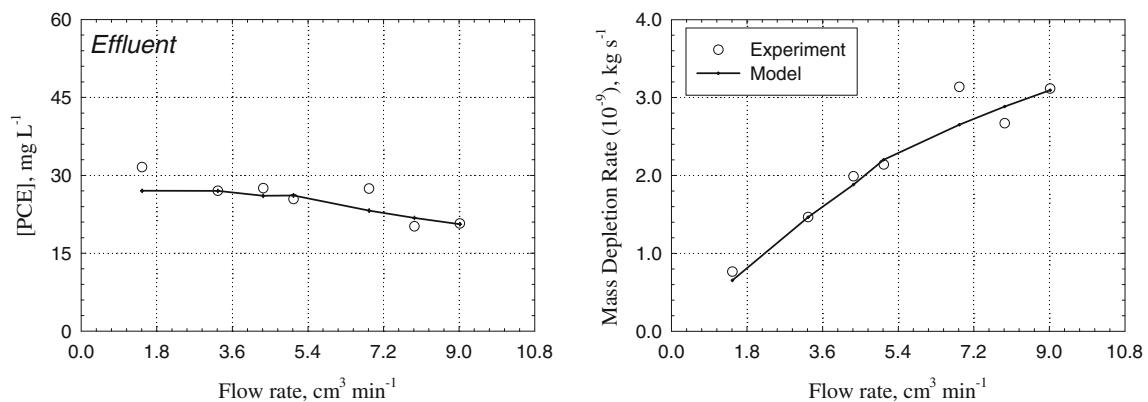


**Fig. 4** Steady-state dissolution of PCE as a function of flow rates: experimental data and model simulated values

Aqueous samples were taken every 30 min until the PCE concentration reached steady-state values. In general, as the flow rate increased, the effluent concentration decreased (Fig. 4). This indicates that dissolution behavior was rate limited and, to some extent, dilution occurred at higher flow rates. However, the steady-state mass depletion rate, which is the product of the steady-state concentration in the effluent and the total flow rate, increased almost linearly with flow rate (Fig. 4). As seepage velocity increased, the rate of mass depletion also increased suggesting that the modified Sherwood number that represents the mass transfer rate was proportional to the Reynolds number (Bird et al. 1960; Miller et al. 1990; Powers et al. 1994).

#### Enhanced dissolution

In the surfactant-enhanced dissolution experiment, a surfactant solution of a concentration  $50 \text{ g L}^{-1}$  concentration (or 5 %) was prepared from concentrated Tween-80. The surfactant solution was injected into the dissolution cell that was flowing at a steady-state of  $8.16 \text{ cm}^3 \text{ min}^{-1}$ . Injection was through three ports located upstream of the

source zone with a combined injection rate of  $2.77 \text{ cm}^3 \text{ min}^{-1}$ . Injection duration was 865 min (14.4 h) and the concentration of PCE was monitored downstream. The PCE concentration at port #5 and the effluent as a function of time for the *first* surfactant flush are shown in Fig. 5. Based on the observed effluent concentration and mass balance, Tween-80 effectively removed some PCE free phase from the source zone. This was confirmed by comparing the resultant steady-state effluent concentration before and after the surfactant flush which decreased from 27.0 to 17.0  $\text{mg L}^{-1}$ . These surfactant-flushing experimental data were used to calibrate the surfactant-enhanced dissolution numerical model which is described in Sect. 4.3. A mass balance calculation using data from the effluent showed that the first surfactant flush removed  $5.67 \text{ cm}^3$  (or 18.3 %) of free-phase PCE.

After the first surfactant injection experiment, the test cell was flushed with two pore volumes of deionized water to remove surfactant residuals and to obtain the steady-state concentration of PCE in the effluent. Then, a second surfactant flushing was initiated. These alternate processes were repeated four times. The surfactant injection durations for the four cycles were 14.4, 15.1, 15.3, and 30.0 h,

respectively. The mass of PCE left in the system was calculated based on the mass balance monitored in the effluent. Figure 6 shows steady-state concentration of PCE

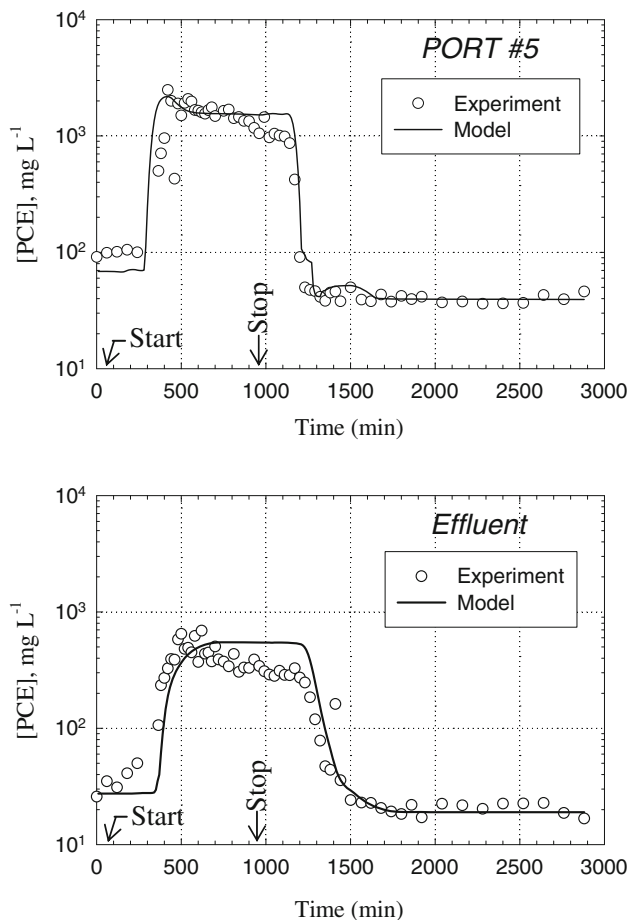


**Fig. 5** Transient, enhanced dissolution of PCE: Experimental data and model simulated values

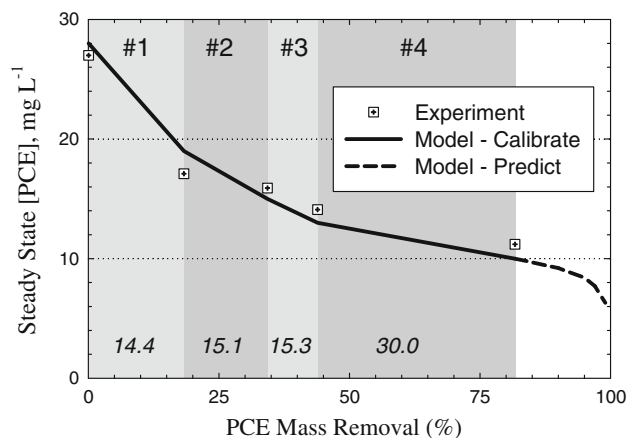


**Fig. 6** Steady-state PCE concentration at the effluent as a function of percent mass removal for four surfactant injections: experimental data versus model calibration and prediction. Duration for each surfactant flush was indicated (14.4, 15.1, 15.3, and 30.0 h)

plotted against the percent of PCE mass removed. As the number of treatment cycles increase, more PCE mass is removed from the source zone. However, the steady-state PCE concentration in the effluent did not drop at the same rate as mass removal. This suggests that, even in this simple DNAPL entrapment system, it is necessary to remove a large amount of free-phase PCE in order to significantly lower the observed PCE concentration downstream. This finding confirms the conclusion made by Sale and McWhorter (2001).

Numerical model calibration

Natural dissolution

Both steady-state and transient dissolution data from dissolution experiments conducted at various effluent flow rates were used in the model calibration. A large amount of data were used as observations in regression analysis in an effort to assure that the calibrated dissolution model with optimized parameters would be able to simulate transient and steady-state natural dissolution over a wide range of hydrodynamic conditions. The calibrated parameters were the empirical coefficients ( $\alpha_1, \alpha_2, \dots, \alpha_4$ ) that appear in Eq. (2). Normal dissolution of PCE was simulated using the dissolution module that was described earlier in Sect. 3.

Hydraulic and aquifer properties as well as model discretization for the dissolution model setup are shown in Table 4. The tortuosity factor used to correct the actual flow path length was set as  $\tau = 2.0$ , suggested by Saba (1999) for sands used in our laboratory. The dissolution or characteristic length in this numerical simulation is the length of the contaminated numerical grid block in the general flow direction.

**Table 4** Model parameters used in natural and surfactant-enhanced dissolution simulations

Parameters	Value	Unit
$\Delta x = \Delta y = \Delta z$	1.0	cm
Number of columns	54	–
Number of rows	45	–
Number of layers	5	–
$K_s$ (#70)	0.81 <sup>a</sup>	cm min <sup>-1</sup>
$K_s$ (#16)	25.8 <sup>a</sup>	cm min <sup>-1</sup>
Porosity (#70)	0.45 <sup>a</sup>	–
Porosity (#16)	0.48 <sup>a</sup>	–
Longitudinal dispersivity	0.035 <sup>a,b</sup>	cm
Transverse dispersivity	0.028 <sup>a,b</sup>	cm

<sup>a</sup> Based on inverse modeling study using conservative tracers breakthrough curves data (Saenton 2003)

<sup>b</sup> Micro-scale dispersivity



**Table 5** Optimized empirical parameters with their 95 % confidence interval and composite-scaled sensitivities for normal dissolution (Eq. 2)

Parameters	Value $\pm$ 95 % CI	Sensitivity
$\alpha_1$	12.41 $\pm$ 0.71	105.7
$\alpha_2$	0.23 $\pm$ 0.02	159.0
$\alpha_3$	0.5	–
$\alpha_4$	1.28 $\pm$ 0.28	127.4

Prior to running a regression (i.e., inverse modeling), the dissolution model was coupled with the inverse modeling algorithm UCODE (Poeter and Hill 1998) (Phase 2) to evaluate the parameters' sensitivities. The sensitivity for parameter  $\alpha_3$  was very small compared to the rest of parameters. This could be due to the fact that the Schmidt number  $Sc = \mu_w / \rho_w D_m$  was relatively constant throughout the simulation. Therefore, it was arbitrarily set constant at  $\alpha_3 = 0.5$  (Miller et al. 1990; Saba et al. 2001). The value of Schmidt number exponent ( $\alpha_3$ ) reported in literature based on both theoretical and experimental studies is in the range of 0.33–0.67 (see references in Khachikian and Harmon 2000). Experimental investigations and theoretical models at high mass transfer rates support this suggestion (Incropera and Dewitt 1985). Thus, only three parameters were left to be estimated. Once the regression converged, UCODE generated a linear 95 % confidence interval (CI) as well as sensitivity for each parameter. Table 5 represents the fitted or optimized empirical coefficients of the dissolution model with their linear 95 % confidence intervals as well as sensitivities of the final parameter values.

The sensitivity of the Reynolds number exponent,  $\alpha_2$ , was highest among the three parameters and this reflected the strong dependence of the mass transfer rate on hydrodynamic conditions. The last term in Eq. (2) or  $(\theta_n d_{50} / \tau L^*)$  that represents pore geometry in the finite-difference grid block had a relatively high sensitivity for its exponent,  $\alpha_4$ , and this reflected the relative importance of the NAPL morphology in mass transfer. The UCODE-generated correlation coefficient ( $r$ ) matrix indicated that there was no significant correlation among the three parameters (i.e., all  $r$ 's  $<$  0.75) and this implied the independence of the parameters from one another. Figures 3 and 4 illustrate examples of the experimental data and the model fit for steady-state and transient dissolution under natural conditions. As can be seen from these figures, the natural dissolution model was able to capture the mass transfer characteristic well.

#### Enhanced dissolution

Similar to natural dissolution, the surfactant-enhanced dissolution option in the dissolution module must also be

**Table 6** Optimized empirical parameters with their 95 % confidence interval and composite-scaled sensitivities for enhanced dissolution (Eq. 3)

Parameters	Value $\pm$ 95 % CI	Sensitivity
$\beta_1$	0.53 $\pm$ 0.11	132.2
$\beta_2$	1.87 $\pm$ 0.46	207.1
$\beta_3$	0.5	–
$\beta_4$	0.19 $\pm$ 0.04	319.6
$\beta_5$	0.20 $\pm$ 0.09	41.2

calibrated. The simulation of enhanced dissolution, however, required mass transfer coefficients for both normal and enhanced conditions. This was because during surfactant injection, the surfactant solution bypassed some numerical grid blocks due to a permeability contrast. In these grid blocks, dissolution occurred under natural conditions. Optimized parameters obtained from Sect. 4.3.1 were used for calculating mass transfer coefficients under natural conditions. Therefore, the calibrated parameters are  $\beta_1, \beta_2, \dots, \beta_5$ , the same that appear in Eq. (3). The transient breakthrough curves shown in Fig. 5 were used for model calibration.

The numerical model setup used the same discretized finite-difference grid system as in the natural dissolution simulation (Table 4). Once the forward simulation executed successfully, the UCODE program (Phase 2) was used to calculate parameter sensitivities. Results were similar to natural dissolution simulation. Sensitivity for the Schmidt number exponent  $\beta_3$  was extremely small compared to other parameters, and it is therefore set as  $\beta_3 = 0.5$ .

It is interesting that the sensitivity for  $\beta_4$ , the exponent for  $\theta_n / (1 - \theta_n)$  term, was highest among the four calibrated parameters. This could be explained by a rapid change in volumetric NAPL content during enhanced dissolution in the presence of surfactant as PCE solubility increased significantly. This analysis confirms the finding by Saba et al. (2001). The rapid change in volumetric NAPL content (or NAPL saturation) also modified the groundwater flow field and, as a result, the Reynolds number exponent became the second largest sensitive parameter.

Once the sensitivity for parameters was determined to have the same order of magnitude by modifying weights of observations, the regression was performed using UCODE (Phase 3). Figure 5 shows examples of experimental data and model simulated, best-fit values for PCE concentration measured at port #5 and the effluent port. The final or optimized parameters with their 95 % confidence interval and the composite-scaled sensitivities are listed in Table 6.

As shown in Fig. 5, the calibrated enhanced dissolution model simulated the surfactant-flushing breakthrough

curves relatively well. No significant correlation was found among parameters except  $\beta_2$  and  $\beta_4$ , where the correlation coefficient was  $r = 0.74$ . This could be explained by the fact that the groundwater flow velocity described in terms of the Reynolds number is closely related to the volumetric NAPL content  $\theta_n$  in the grid block. Figure 6 shows the model's capability to simulate the effect of partial source zone treatment where PCE is partially removed from the source zone. The dashed line represents the model prediction that implies almost complete removal (>99 %) of entrapped DNAPL was required in order to lower the downstream concentration to the MCL.

Based on the numerical modeling presented in this section, we obtained a calibrated mass transfer model that can be used to predict mass transfer from this particular source zone. This dissolution model is able to simulate the dissolution of entrapped PCE ranging from residual to pool saturation for  $10^{-4} \leq Re \leq 10^{-2}$ : a typical natural groundwater flow condition. It is, however, expected that the constitutive relationships as shown in Eqs. (2) and (3) can be extrapolated to conditions outside the reported range.

### Numerical simulations study of partial source zone treatment

The goal of this numerical simulation experiment was to evaluate the effect on the downstream plume concentration of partial removal of NAPL mass from the source zone that was observed in the experiments. The approach was to conduct Monte Carlo-based numerical experiments using 80 hypothetical heterogeneous aquifers containing PCE distributions created from spill simulations with UTCHEM. These hypothetical aquifers were similar to those used in the study by Saenton and Illangasekare (2007).

### Intermediate-scale test aquifer

A set of 80 numerical simulations was conducted to represent conditions in a 2-D intermediate-scale, heterogeneously packed test aquifer with the dimensions of 9.5 m long 1.0 m high and 5.0 cm thick. The test aquifer consists of homogeneous and heterogeneous zones (Fig. 7). The numerical simulation was conducted after an earlier experimental study by Barth (1999) and Barth et al. (2001a, b). Two constant head boundaries are used to maintain a steady hydraulic gradient throughout the test aquifer. The homogeneous area of the test aquifer consists of #8 sand. A fully penetrated injection well is placed in this homogeneous area to deliver a treating agent for NAPL mass removal by enhanced dissolution. The heterogeneous zone is packed using five sands of different sieve sizes (#16, #30, #50, #70, and #110). The properties of these sands are listed in Table 3.

The heterogeneity was designed as a spatially correlated random field with statistical parameters similar to heterogeneous field sites. This heterogeneous packing assumed a log-normal distribution of hydraulic conductivity with  $\ln K_s$  of 4.18 ( $K_s$  is in  $\text{cm h}^{-1}$ ) and a variance  $s_{\ln K_s}^2$  of 1.22. The correlation lengths in lateral ( $\lambda_h$ ) and vertical ( $\lambda_v$ ) directions were 50.8 and 5.08 cm, respectively. The heterogeneous zone consisted of 1,280 cells of 25.4 cm in length and 2.54 cm in depth. The 32 columns and 40 layers resulted in 16 lateral and 20 vertical correlation lengths. A more detailed discussion of tank setup and packing can be found in Barth (1999) and Barth et al. (2001a, b).

### DNAPL source zone

The NAPL source zone ( $1.6 \times 1.0 \times 0.05 \text{ m}^3$ ) was created from a spill simulation using UTCHEM while all subsequent mass transfer simulations were conducted using MODFLOW/RT3D described in Sect. 3. The location of

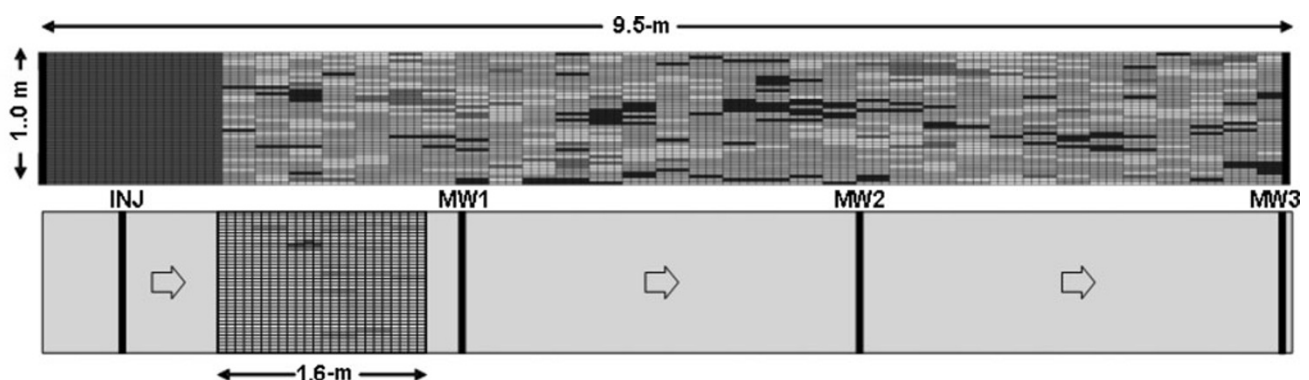


**Fig. 7** Heterogeneous test tank (hypothetical) used in this numerical modeling investigation. *Darker color* indicates higher hydraulic conductivity

the source zone is shown in Fig. 7. The source zone was discretized into 1 row, 40 layers and 24 columns. The Brooks–Corey model (1966) was used to represent the capillary pressure–saturation relationship. Total PCE spill volume was 1.0 L, the average saturation was  $\bar{S}_n = 0.036$ , and the spill rate was  $1.67 \text{ L day}^{-1}$ . The spill location was placed at the center of the top layer. The spill simulation was executed until the spill, or migration of PCE reached a static state. Note that in all simulations, the finest sand (#110) was replaced with clay in order to generate a realistic impermeable barrier that could be encountered during DNAPL migration in the field soils.

Three PCE source zone architectures were selected for this study: realization #1 (Spill 01), realization #2 (Spill 11), and realization #54 (Spill 54). Examples of the resulting simulated PCE distribution are illustrated in Fig. 8. As can be seen from the distribution pattern, the PCE source zone consisted of both high saturation pools and residual zones. In realization #54, most of the spilled PCE formed pools on top of clay lenses. On the other hand, most PCE in Spill 11 was entrapped from intermediate to low saturation zones. However, realization #1 shows that both high saturated pools and residual zones are found throughout the depth of the source zone. Saenton and Illangasekare (2007) quantified these source zones using the spatial moment analysis of mass distribution and showed that entrapment architecture is an important parameter controlling mass transfer and, hence, mass fluxes and source longevity.

#### Surfactant-enhanced remediation simulation

This section investigates the effect of partial source zone treatment on the reduction of the contaminant concentration level at a compliance plane or monitoring well located downstream. Instead of arbitrarily removing the mass from the source zone, the surfactant technology was selected because it effectively and rapidly removes free-phase NAPL. More importantly, the effect of flow bypassing due to a hydrodynamic constraint can be included in the analysis.

In surfactant-enhanced remediation simulation, a fully penetrated extraction well was placed at the downstream end of the source zone (i.e., same location as monitoring well #1). A surfactant solution containing Tween-80 at a concentration of  $50.0 \text{ g L}^{-1}$  was continuously injected upstream of the source zone through a fully penetrated injection well at the flow rate of  $1.60 \text{ cm}^3 \text{ min}^{-1}$ . This flow rate is approximately 60 % of the total steady-state groundwater flow rate of the tank under a constant hydraulic gradient of  $10^{-3}$ .

Mass of the PCE remaining in the source zone as a function of treatment time for all realizations is shown in Fig. 9. Simulation results showed a large variation (or uncertainty) in mass depletion rates for the 80 simulations.

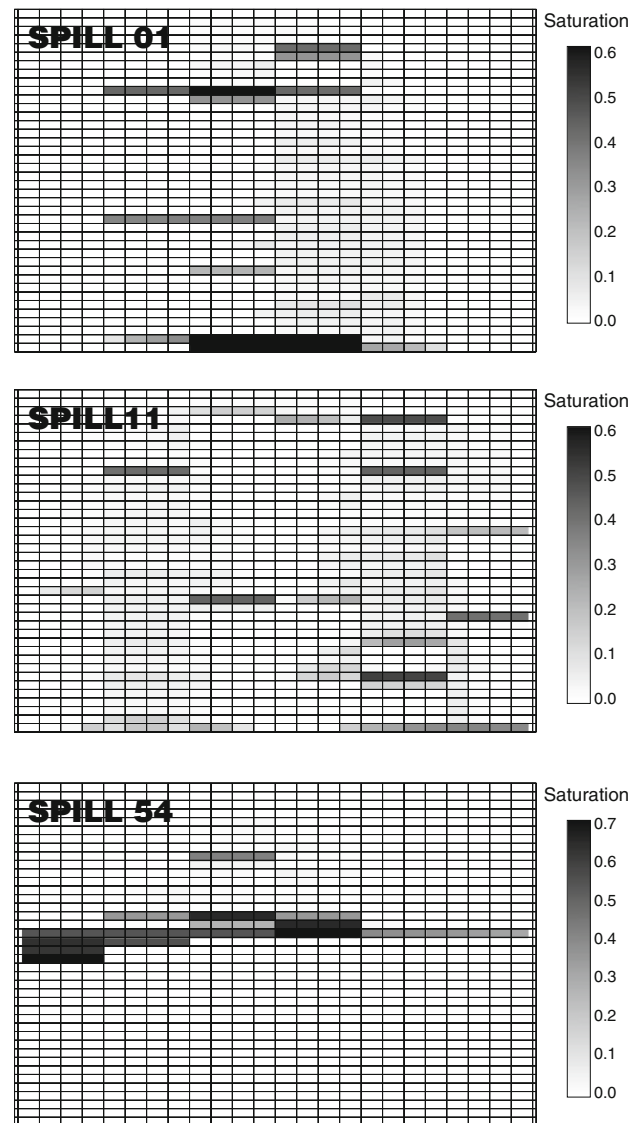
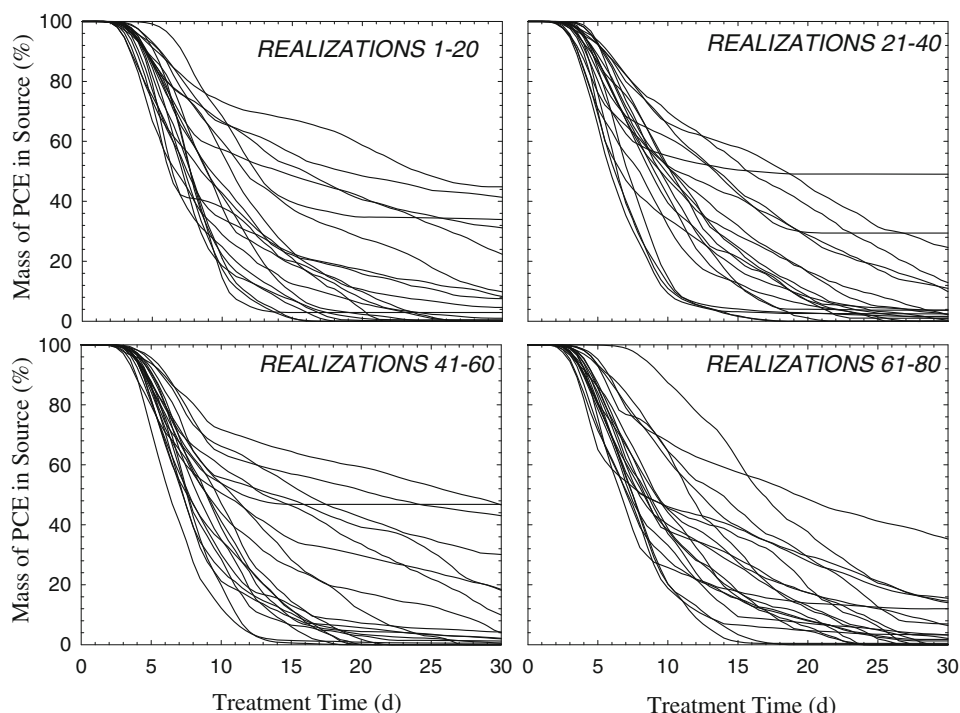


**Fig. 8** PCE distribution in the source zone for realization #1, 11, and 54 (Saenton and Illangasekare 2007)

Although all the breakthrough curves are smooth, the non-constant slopes indicate different mass removal rates from different zones of entrapped PCE. In some cases, PCE mass removal rate was high and PCE mass rapidly dropped soon after the surfactant solution attacked the free-phase PCE. However, in most cases, it took some time to extract PCE mass from the source zone. This is due to the fact that surfactant-enhanced dissolution is rate limited. Permeability contrasts resulted in flow bypassing and limited full contact of the free-phase PCE with the surfactant solution.

There are a few interesting cases where the mass reduction rate was nearly zero as indicated in Fig. 9 by nearly horizontal % mass lines. After significant removal of the easily accessible entrapped PCE mass, high saturation entrapped PCE in the pool was completely bypassed by the

**Fig. 9** Mass of PCE in the source zone as a function of cleanup time using surfactant



flowing groundwater. Despite a relatively large PCE mass fraction remaining in the source, natural dissolution resulted in an insignificant amount of dissolved mass flux or concentration.

To further investigate the benefits of partial source zone treatment, stepwise injection of the surfactant solution was conducted. The procedure was similar to what was used in the experiment. After injecting surfactant solution of duration  $\Delta t_i$ , PCE mass of  $\Delta m_i$  was removed from the source zone. Then, the aquifer was relaxed (i.e., no surfactant injection) and the natural dissolution model was used to simulate the steady-state PCE concentration in the monitoring well  $c_i$  under the normal hydraulic gradient of  $10^{-3}$ . This steady-state PCE concentration  $c_i$  was recorded as a function of percent mass removal or  $(m_0 - \Delta m_i)/m_0$ , where  $m_0$  is the original mass of PCE in the source zone. These alternate processes were repeated until the mass removal was close to completion or  $(m_0 - \Delta m_i)/m_0 \rightarrow 0$ .

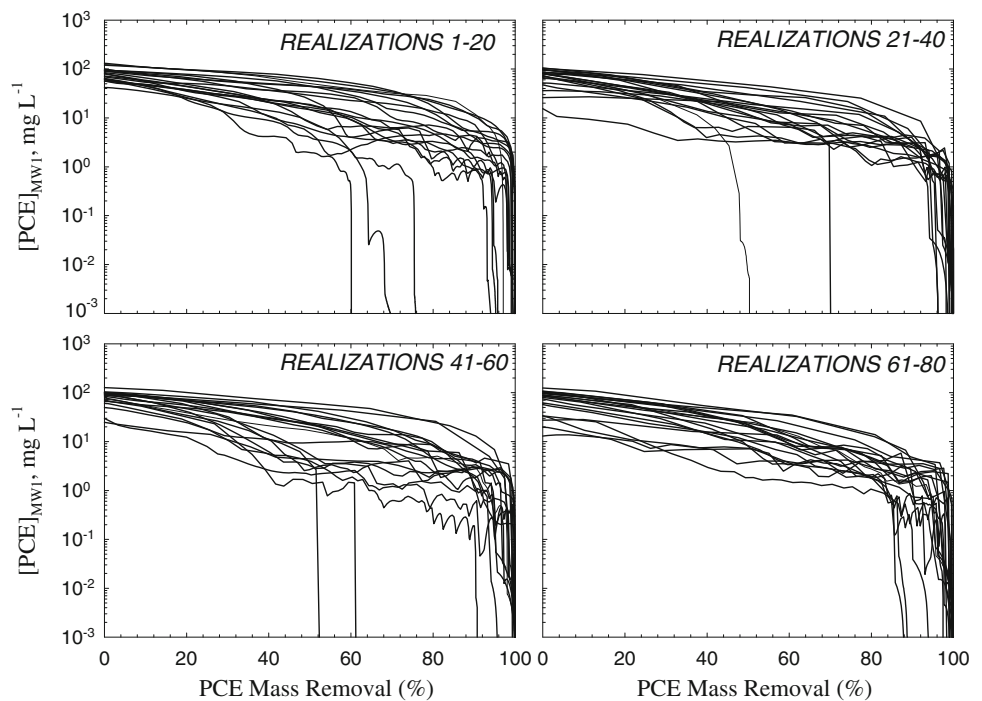
Figure 10 shows the steady-state PCE concentration at monitoring well 1 (MW1) as a function of percentage mass removal. In most cases, it was necessary to remove at least 80 % of the total PCE mass from the source zone to observe any significant concentration drop in the downstream plume. More than 99 % of the total mass had to be removed in order to lower the plume concentration below the maximum concentration limit (MCL) of  $5.0 \mu\text{g L}^{-1}$ . However, a few exceptions to this rule are found in some realizations. These realizations contained a high saturation DNAPL pool located beneath a high permeability layer. As a result, groundwater nearly completely bypassed these

NAPL containing grid blocks, and dissolved mass flux or concentration from the pools became insignificant. The numerical results based on 80 realizations of the spatially correlated hydraulic conductivity field agreed conceptually with the experimental results shown in Fig. 6. The removal of entrapped DNAPL based on the injection of treating reagents is largely controlled by the success in delivery through groundwater flow.

## Conclusions

This study investigated the effects of partial removal of NAPLs from source zones. A previous investigation by Sale and McWhorter (2001) pointed out the limited near-term benefits of partial source zone treatment in achieving cleanup goals. The conclusions of their study could not be generalized because of simplifying assumptions that were made with respect to the source architecture and flow field. Our study presented a methodology that used experimentally validated numerical models that simulate natural and enhanced dissolution in heterogeneous aquifers where NAPLs are entrapped in complex architecture. Results based on 80 realizations suggest that a very large fraction of NAPL mass has to be removed from the source zone to make any significant impact on the plume concentrations downstream of the source zone. However, this study and Saenton et al. (2002) demonstrate that source zone cleanup technologies which involve the delivery of treating chemicals (e.g., surfactants) may not be as effective as expected

**Fig. 10** Steady-state PCE concentration in MW1 as a function of mass of PCE removed from the source zone



because the ability to fully deliver these reagents is hindered by the bypassing effect.

**Acknowledgments** The authors gratefully acknowledge the following funding sources: (1) National Science Foundation Major Research Instrumentation Award BES-997708, (2) National Science Foundation Award EAR-0107095, (3) Department of Defense SER-DP Grant CU-1294, and (4) Faculty of Science, Chiang Mai University. Special thanks to Dr. Gilbert R. Barth who provided the spatially correlated hydraulic conductivity fields.

**Open Access** This article is distributed under the terms of the Creative Commons Attribution License which permits any use, distribution, and reproduction in any medium, provided the original author(s) and the source are credited.

## References

- Abdul A, Gibson T, Ang C, Smith J (1992) In situ surfactant washing of polychlorinated biphenyls and oils from contaminated soils. *Groundwater* 30:219–231
- Barth G (1999) Intermediate-scale tracer tests in heterogeneous porous media: Investigation of density, predictability and characterization of NAPL entrapment, Ph.D. thesis, University of Colorado, Boulder Colorado, USA
- Barth G, Hill M, Illangasekare T, Rajaram H (2001a) Predictive modelling of flow and transport in a two-dimensional intermediate-scale, heterogeneous porous medium. *Water Resour Res* 37(10):2503–2512
- Barth G, Illangasekare T, Hill M, Rajaram H (2001b) A new tracer-density criterion for heterogeneous porous media. *Water Resour Res* 37(1):21–31
- Basu N, Rao PSC, Falta RW, Annable MD, Jawitz JW, Hatfield K (2008) Temporal evolution of DNAPL source and contaminant-flux distribution: impacts of source mass depletion. *J Contam Hydrol* 95:93–109
- Bird R, Stewart E, Lightfoot E (1960) *Transport Phenomena*. John Wiley, New York
- Bradford S, Phelan T, Abriola L (2000) Dissolution of residual tetrachloroethylene in fractional wettability porous media: correlation development and application. *J Contam Hydrol* 45(1–2):35–61
- Brooks RH, Corey AT (1966) Properties of porous media affecting fluid flow. *J Irrig Drain Eng* 92(2):61–88
- Brusseau ML, DiFilippo EL, Marble JC, Oostrom M (2008) Mass-removal and mass-flux-reduction behavior for idealized source zones with hydraulically-poorly-accessible immiscible liquid. *Chemosphere* 71(8):1511–1521
- Clement T (1997) RT3D: a modular computer code for simulating reactive multiple species transport in 3-dimensional groundwater systems
- Compos R (1998) Hydraulic conductivity distribution in a DNAPL entrapped zone in a spatially correlated random field. Master's Thesis, University of Colorado, Boulder, CO, USA
- Dekker T, Abriola L (2000) The influence of field-scale heterogeneity on the infiltration and entrapment of dense non-aqueous phase liquids in saturated formations. *J Contam Hydrol* 42:187–218
- Delshad M, Pope G, Sepehrnoori K (1996) A compositional simulator for modelling surfactant enhanced aquifer remediation. *J Contam Hydrol* 23(1–2):303–327
- DiFilippo EL, Brusseau ML (2011) Assessment of a simple function to evaluate the relationship between mass flux reduction and mass removal for organic-liquid contaminated source zones. *J Contam Hydrol* 123:104–113
- Ewing J (1996) Effects of dimensionality and heterogeneous on surfactant-enhanced solubilization of non-aqueous phase liquids in porous media, Master's thesis, University of Colorado, Boulder, CO, USA
- Falta RW, Rao PS, Basu N (2005) Assessing the impacts of partial mass depletion on DNAPL source zones I. Analytical modeling of source strength functions and plume response. *J Contam Hydrol* 78(4):259–308
- Fountain J, Klimek A, Beikirch M, Middleton T (1991) Use of surfactants for in situ extraction of organic pollutants from a contaminated aquifer. *J Hazard Mat* 38(3):295–311

- Grant GP, Gerhard JJ, Kueper BH (2007) Multidimensional validation of a numerical model for simulating a DNAPL release in heterogeneous porous media. *J Contam Hydrol* 92:109–128
- Harbaugh A, Banta E, Hill M, and McDonald M (2000) MODFLOW-2000, the US Geological Survey modular ground-water model—user guide to modularization concepts and the ground-water flow process, Open-File Report 00-92, US Geological Survey
- Illangasekare T (1998) Flow and entrapment of non-aqueous phase liquids in heterogeneous soils formations. In: Selim HM and Ma L (eds), *Physical Non-equilibrium in Soil*. Ann Arbor Press, Chelsea, Michigan, pp 417–423
- Illangasekare T, Ramsey J, Jensen K, Butts M (1995) Experimental study of movement and distribution of dense organic contaminants in heterogeneous aquifers: an experimental study. *J Contam Hydrol* 20(1):1–25
- Imhoff P, Jaffe P, Pinder G (1994) An experimental study of complete dissolution of a non-aqueous phase liquid in saturated porous media. *Water Resour Res* 30(2):307–320
- Incropera FP, Dewitt DP (1985) *Fundamentals of heat and mass transfer*. Wiley, New York
- Kaluvarachchi J, Parker J (1990) Modelling multi-component organic chemical transport in three-phase porous media. *J Contam Hydrol* 5:349
- Khachikian C, Harmon TC (2000) Non-aqueous phase liquid dissolution in porous media: current state of knowledge and research needs. *Transp Porous Media* 38(1):3–28
- Kueper B, Frind E (1991) Two-phase flow in heterogeneous porous media: 2. Model application. *Water Resour Res* 27(6):1059–1510
- Kueper B, Gerhard J (1995) Variability of point source infiltration rates for two-phase flow in heterogeneous porous media. *Water Resour Res* 31(12):2971–2980
- Kueper B, Abbot W, Farquhar G (1989) Experimental observations of multiphase flow in heterogeneous porous media. *J Contam Hydrol* 5(1):83–95
- Lucius J, Olhoeft G, Hill P, and Duke S (1992) *Properties and Hazards of 108 Selected Substances*, US Geological Survey, Open-File Report 92-527, September
- Martel R, Gelinas P, Saumure L (1998) Aquifer washing by micellar solutions: 3. Field test at the Thouin sand pit. *J Contam Hydrol* 30:33–48
- Mason A, Kueper B (1996) Numerical simulation of surfactant-enhanced solubilization of pooled DNAPL. *Environ Sci Technol* 30(11):3205–3226
- Maji R and Sudicky GA (2008) Influence of mass transfer characteristics for DNAPL source depletion and contaminant flux in a highly characterized glaciofluvial aquifer. *J Contam Hydrol* 102:105–119
- McCray J, Brusseau M (1998) Cyclodextrin-enhanced in situ flushing of multiple-component immiscible organic liquid contamination at the field scale: mass removal effectiveness. *Environ Sci Technol* 32(9):1285–1293
- McCray J, Bai G, Maier R, Brusseau M (2001) Biosurfactants-enhanced solubilization of NAPL mixtures. *J Contam Hydrol* 48(1):45–68
- Meinardus HW, Dwarakanath V, Ewing J, Hirasaki GJ, Jackson RE, Jin M, Ginn JS, Londergen JT, Miller CA, Pope GA (2002) Performance assessment of NAPL remediation in heterogeneous alluvium. *J Contam Hydrol* 54:173–193
- Mercer J, Cohen R (1990) A review of immiscible fluids in the subsurface: properties, models, characterization and remediation. *J Contam Hydrol* 6:107–163
- Miller C, Poirier-McNeil M, Mayer A (1990) Dissolution of trapped non-aqueous phase liquids: mass transfer characteristics. *Water Resour Res* 23(11):2783–2793
- Nambi I, Powers S (2000) NAPL dissolution in heterogeneous systems: an experimental investigation in a simple heterogeneous system. *J Contam Hydrol* 44:168–184
- Nelson N, Oostrom M and Brusseau TWM (1999) Partitioning tracer method for the in situ measurement of DNAPL saturation: influence of heterogeneity and sampling method. *Environ Sci Technol* 33(22):4046–4053
- Park E, Parker JC (2005) Evaluation of an upscaled model for DNAPL dissolution kinetics in heterogeneous aquifers. *Adv Water Resour* 28(12):1280–1291
- Parker JC, Park E (2004) Modeling field-scale dense nonaqueous phase liquid dissolution kinetics in heterogeneous aquifers. *Water Resour Res* 40:05109. doi:10.1029/2003WR002807
- Pennell K, Abriola L, Weber W Jr (1993) Surfactant enhanced solubilization of residual dodecane in soil columns: 1. Experimental investigation. *Environ Sci Technol* 27(12):2332–2340
- Pennell K, Abriola L, Pope G (1994) Surfactant enhanced remediation of soil columns contaminated by residual tetrachloroethylene. *J Contam Hydrol* 16(1):35–53
- Poeter E, and Hill M (1998) Documentation of UCODE, a computer code for universal inverse modelling, Water-Resources Investigation Report 98-4080, US Geological Survey
- Powers S, Abriola L, Weber W Jr (1992) An experimental investigation of non-aqueous phase liquid dissolution in saturated subsurface systems: steady state mass transfer rates. *Water Resour Res* 28(10):2691–2705
- Powers S, Abriola L, Weber W Jr (1994) An experimental investigation of non-aqueous phase liquid dissolution in saturated subsurface systems: transient mass transfer rate. *Water Resour Res* 30(1):321–333
- Rathfelder K, Abriola L, Taylor T, Pennell K (2001) Surfactant enhanced recovery of tetrachloroethylene from a porous medium containing low permeability lenses: 2. Numerical simulation. *J Contam Hydrol* 48:351–374
- Saba T (1999) Up-scaling of mass transfer from entrapped NAPLs under natural and enhanced conditions, Ph.D. thesis, University of Colorado, Boulder, CO, USA
- Saba T, Illangasekare T (2000) Effect of ground-water flow dimensionality on mass transfer from entrapped non-aqueous phase liquid contaminants. *Water Resour Res* 36(4):971–979
- Saba T, Illangasekare T, Ewing J (2001) Surfactant enhanced dissolution entrapped NAPLs in multidimensional flow fields. *J Contam Hydrol* 51(1–2):63–82
- Saenton S (2003) Prediction of mass flux from DNAPL source zone with complex entrapment architecture: Model development, experimental validation, and up-scaling, Ph.D. thesis, Colorado School of Mines, Golden, CO, USA
- Saenton S, Illangasekare TH (2007) Up-scaling of mass transfer rate coefficient for the numerical simulation of DNAPL dissolution in heterogeneous aquifers. *Water Resour Res* 43:W02428
- Saenton S, Illangasekare T, Soga K, Saba T (2002) Effect of source zone heterogeneity on surfactant enhanced NAPL dissolution and resulting remediation endpoints. *J Contam Hydrol* 53(1–2):27–44
- Sale T, McWhorter D (2001) Steady-state mass transfer from single-component dense non-aqueous phase liquids in uniform flow fields. *Water Resour Res* 37(2):393–404
- Schaerlaekens J, Feyen J (2004) Effect of scale and dimensionality on the surfactant enhanced solubilization of residual DNAPL contamination. *J Contam Hydrol* 71:283–306
- Sleep B, Sykes J (1993) Compositional simulation of groundwater contamination by organic compounds. *Water Resour Res* 29(6):1697–1708
- US Environmental Protection Agency (EPA) (1996) *Soil screening guidance: technical background document*, EPA/540/R-95/128, July
- van Genuchten MT (1980) A closed-form equation for predicting the hydraulic conductivity of unsaturated soils. *Soil Sci Soc Am J* 44:892–898
- Wyllie M (1962) *Relative permeability in petroleum production handbook, reservoir engineering*, vol 11. McGraw-Hill, New York

